Electronic structure of imperfect Si/Ge heterostructures

M. J. Shaw, P. R. Briddon, and M. Jaros
Department of Physics, The University of Newcastle upon Tyne, Newcastle upon Tyne, United Kingdom
(Received 14 June 1996; revised manuscript received 30 July 1996)

Local-density *ab initio* pseudopotential calculations have been carried out to study the electronic structure of imperfect Si/Ge superlattices. The interaction between the interfaces and substitutional defects results in interface-related localized resonances, and causes local perturbations in other states of the heterostructures. In particular, the antimony impurity shows a high degree of coupling to the superlattice. Analogous localization also occurs at germanium atoms replacing host atoms in the silicon layers. [S0163-1829(96)03247-X]

I. INTRODUCTION

There have been numerous studies of ordered Si/Ge heterostructures which led to a detailed picture of the electronic structure and stability.[1] However, the origin of some of the key observables (e.g., optical spectra) is still poorly understood.[2–7] The structures modeled *ab initio* have almost without exception been ''perfect'' in that dopants and/or germanium or silicon interdiffusion into adjacent layers were not accounted for. Yet it is well known that the layers are not perfect. Donors are invariably present in significant concentrations; for example antimony donors are regularly used as a surfactant to improve the layer quality.

In this paper we studied short-period [001] Si/Ge superlattices with substitutional defects close to the interfaces. Local-density *ab initio* pseudopotential calculations were performed to provide the microscopic description of this system, and in particular to model the interaction of the interfaces with the defect atoms. We report a strong interaction between the interfaces and the antimony defects. As a result, the antimony defects create a significant local perturbation to the electronic properties of the Si/Ge heterostructures. We also show that localization occurs at germanium atoms occupying host sites in the silicon layers. This opens a parameter space for both experimentation and modeling in which to achieve a more realistic appreciation of transport and optical properties of Si/Ge structures. We have demonstrated the deep-level signature of the localized states, and shown conclusively the contrasting behavior of the antimony and arsenic defects. Although we established that both the specific chemical properties of the defect ions and the size of the lattice relaxation contribute to the difference in the behavior of the resonances, it would be premature to speculate on the quantitative relation between these two effects. To what extent the difference can be attributed to each of these effects is clearly a question of great importance. However, a systematic investigation of a variety of defects is required in order to make the necessary definitive generalizations. This is indeed the agenda of our current research program.

II. THEORETICAL CONSIDERATIONS

Self-consistent calculations, based upon the local-density approximation of the density-functional theory, are presented, using the *ab initio* pseudopotentials of Bachelet, Hamann, and Schlüter.[8] This method was applied to a periodic system with a unit cell containing 64 atoms. A Gaussian basis set, multiplied by spherical harmonics to obtain s- and p-type functions, was used for the expansion of the wave function. Sixteen of these functions were centered on each atom, together with eight centered on the midbond positions. An intermediate fit to the charge density is also required by our formalism (see, for example, Jones[9]). This formalism has been applied with considerable success to a description of interface-induced localization in AlSb/InAs superlattices.[10] The 64-atom unit cell used describes a Si_4Ge_4 superlattice with eight spirals of atoms in the plane with structures containing a defect modeled by replacing a Si atom adjacent to the interface. A calculation was also performed for an equivalent strained bulk Si with defects. We described these cells using a single wave vector, the Brillouin-zone center—this was found to provide a good representation of the special k points equivalent to the set of ten points frequently used to describe the primitive diamond unit cell. The dimensions of the unit cell in the plane parallel to the interfaces were fixed according to the lattice constant of the substrate used. In the calculations presented here a $Si_{0.5}Ge_{0.5}$ alloy substrate was assumed, with its parallel lattice constant determined from our theoretical values of the bulk Si and Ge lattice constants using the virtual-crystal approximation. The overall length of the unit cell was optimized to minimize the total energy. For each calculation the positions of all of the atoms in the unit cell were fully relaxed.

A simple qualitative picture of a defect in a crystal is provided by the defect molecule model. This is illustrated in Fig. 1. The defect is considered by first removing an atom from the perfect crystal to form a series of vacancy states, then considering the interaction between these states and those of a free defect atom. Considering the case of a defect in bulk, the creation of a vacancy results in four unbonded sp^3 orbitals which symmetrize to form a singlet A_1 state and triplet T_2 state in the gap. The free-atom s (A_1) and p (T_2) orbitals interact with the vacancy states of the same symmetry to form bonding and antibonding pairs. This results in A_1 bonding ($A1B$) and antibonding resonances ($A1A$) near the bottom of the valence and conduction bands, respectively, and T_2 bonding ($T2B$) and antibonding ($T2A$) resonances deep inside the valence and conduction bands. Note that this is a particularly simple model, and neglects completely the interaction between the defect and the

0163-1829/96/54(23)/16781(5)/$10.00 © 1996 The American Physical Society

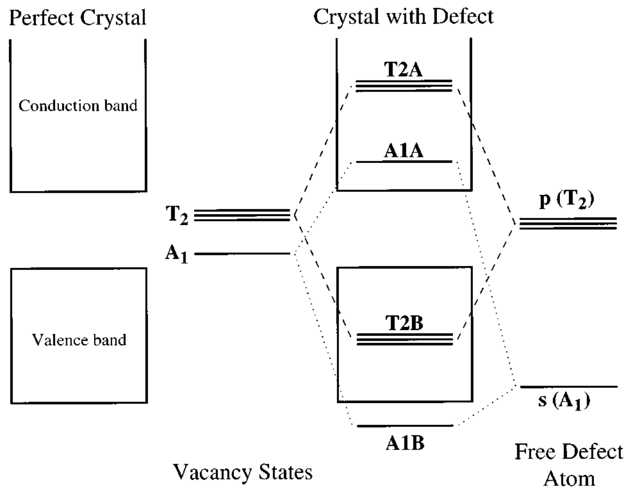

FIG. 1. Schematic diagram representing the simple defect molecule model for a defect in a bulk crystal.

lattice. However, it does describe the qualitative features we expect to find, and provides a framework for the interpretation of the results obtained from our full-scale calculations. For the case of the superlattice structures the symmetry group is different, and strictly speaking we should relabel the resonances according to the C_{2v} group appropriate for the imperfect superlattices. For the purposes of this current work, though, such a refinement is unnecessary, and for clarity we shall apply the same resonance labeling as in the bulk example.

We are not concerned in the present study with the extended features such as the shallow-donor state, lying just below the conduction-band edge, and exciton levels. Rather we concentrate on the localized effects of the defect-interface interaction, particularly the localization of charge in the A_1 antibonding resonance lying close to the conduction-band edge, and the perturbations to the confined superlattice states. In future work, the effect of the interface-related localization on the defect may be projected on to the extended-state wave functions to provide a direct link to the optical and transport properties, and to experiment. However, this lies beyond the scope of this paper.

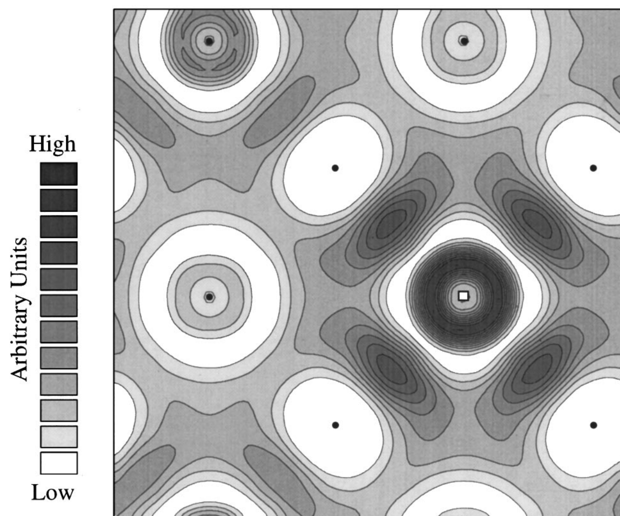

FIG. 2. The charge density (arbitrary units) of the $A1A$ resonance of an antimony defect in strained bulk Si. The plotting plane is parallel to the substrate surface, through the defect atom. The solid circles show projections of the Si atoms which lay in the plane of the defect prior to relaxation, and the open box indicates the defect atom itself.

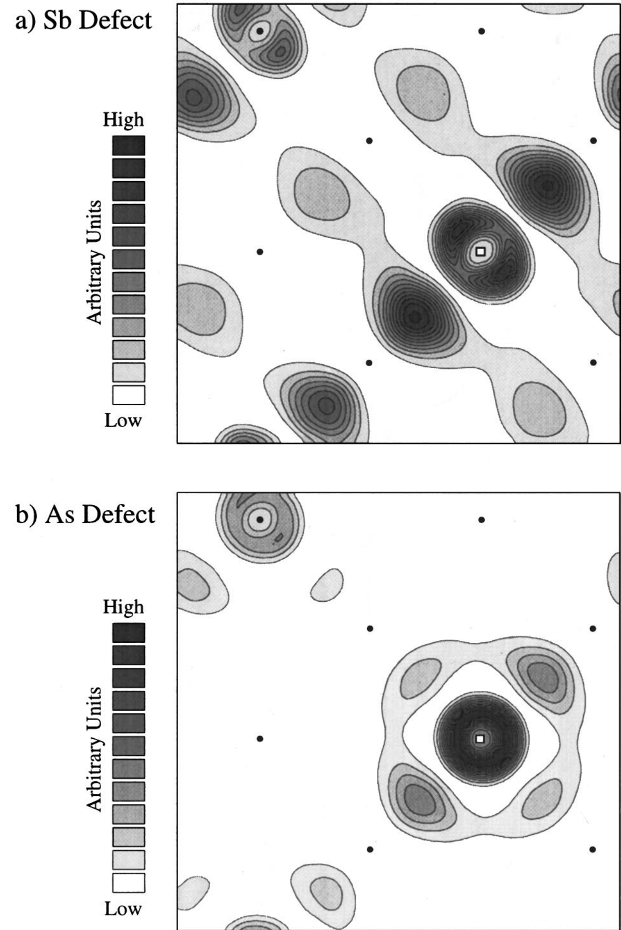

FIG. 3. Charge densities (arbitrary units) of the $A1A$ resonances of (a) antimony and (b) arsenic defects in the Si_4Ge_4 superlattice, plotted in the plane parallel to the interfaces. The solid circles represent projections of the Si atoms which lay in the plotting plane prior to relaxation, and the open box shows the position of the defect atoms.

III. RESULTS

A. Donor resonances

In Fig. 2 the charge density of the $A1A$ resonance is plotted for the case of an antimony defect in bulk Si, strained to a $Si_{0.5}Ge_{0.5}$ alloy substrate. The charge density is plotted in the plane parallel to the surface of the substrate, passing through the defect atom. The positions of the other atoms which were in the plane of the defect before relaxation, and which were found to move only a small distance from the plane, were projected onto the plotting plane, and are indicated by solid circles. This may be compared to Fig. 3(a) where the charge density of the $A1A$ resonance of an antimony defect in a Si_4Ge_4 superlattice is plotted in a comparable plane, parallel to the superlattice interfaces. While the

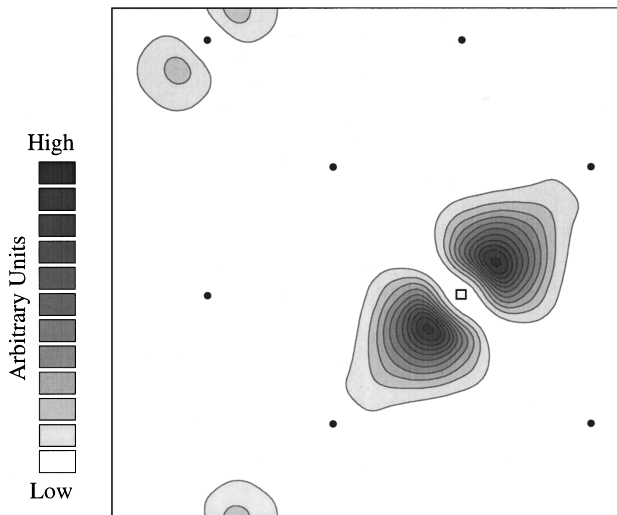

FIG. 4. Charge densities (arbitrary units) of one of the $T2B$ resonances of antimony in the Si_4Ge_4 superlattice, plotted in the plane parallel to the interfaces. The solid circles represent projections of the Si atoms which lay in the plotting plane prior to relaxation, and the open box shows the position of the antimony atom.

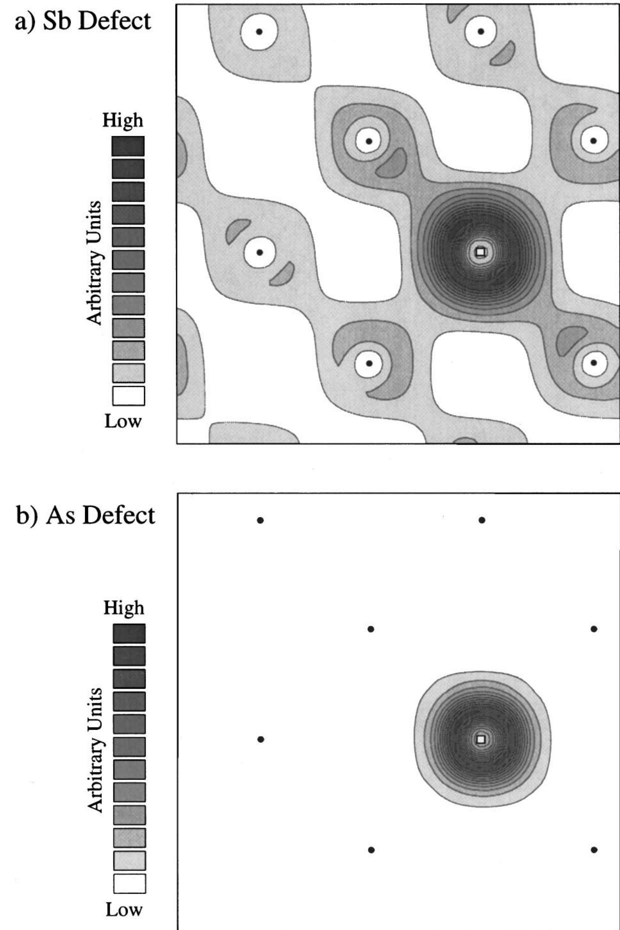

FIG. 5. Charge densities (arbitrary units) of the $A1B$ resonances of (a) antimony and (b) arsenic defects in the Si_4Ge_4 superlattice, plotted in the plane parallel to the interfaces. The solid circles represent projections of the Si atoms which lay in the plotting plane prior to relaxation, and the open box shows the position of the defect atoms.

localized $A1A$ resonance of antimony in bulk Si clearly shows a near-spherical form, the contrast in the case of the superlattice is striking. Here the defect resonance has been strongly perturbed taking on an axial shape. Figures 2 and 3(a) demonstrate the effect the introduction of Si-Ge interfaces has on the charge distribution of the antimony $A1A$ resonance. The formation of this interface-related localized state in the superlattice illustrates the high degree of coupling between the antimony defect and the lattice potential. The antimony defect also gives rise to localized bonding resonances, as predicted by the simple defect molecule model (see Fig. 1). Figure 4 shows the localization of one of the T_2 bonding resonances deep in the valence band, while Fig. 5(a) shows the charge density associated with the A_1 bonding resonance. These lower-energy resonances reflect the modifications to the charge density associated with the bonds between the antimony atom and its neighbors in the interface region.

In addition to the calculation for the antimony defect, we modeled a superlattice structure which included a substitutional arsenic defect. The charge density of the $A1A$ resonance for the superlattice with the arsenic defect is shown in Fig. 3(b), again plotted in the plane parallel to the interfaces and passing through the defect. The arsenic defect is seen to result in an $A1A$ resonance qualitatively similar to the resonance of antimony in bulk Si, but sharply contrasting with the antimony in the superlattice of Fig. 3(a). Thus we see that the large effect resulting from the introduction of the interfaces is peculiar to the antimony defect. While the antimony resonance is clearly strongly influenced by the superlattice interface potential, the arsenic behaves almost independently of its environment. As in the case of the antimony defect, the arsenic introduces lower-energy bonding resonances. By way of example, the charge density of the A_1 bonding resonance is shown in Fig. 5(b). For each defect type the resonances exhibit a localization of the charge extending over a volume containing many atoms. Both defects therefore introduce resonance localization on a length scale capable of inducing a significant change to the superlattice properties.

The results presented demonstrate a clear difference in the behavior of the antimony and arsenic defects. It is not clear whether this difference originates primarily in the differing degrees of lattice relaxation associated with each defect (the relaxation in the vicinity of the antimony being approximately twice that of arsenic), or in the chemical nature of the defect ions themselves. The separation and identification of the roles played by these two effects requires a detailed systematic study of a variety of defect structures. Such a study represents a considerable computational effort, and shall be the subject of a future paper. While here we do not attempt to identify the extent of each effect conclusively , a calculation in which an antimony defect is introduced but where the lattice relaxation is inhibited indicates that the relaxation certainly plays a significant role, greatly lowering the energy of the $A1A$ resonance. The resonances introduced by the antimony and arsenic defects are thus seen to demonstrate the signature of genuine deep levels,[11] further verified by the atomic s-like nature of the charge densities of the A_1 bonding resonances shown in Fig. 5.

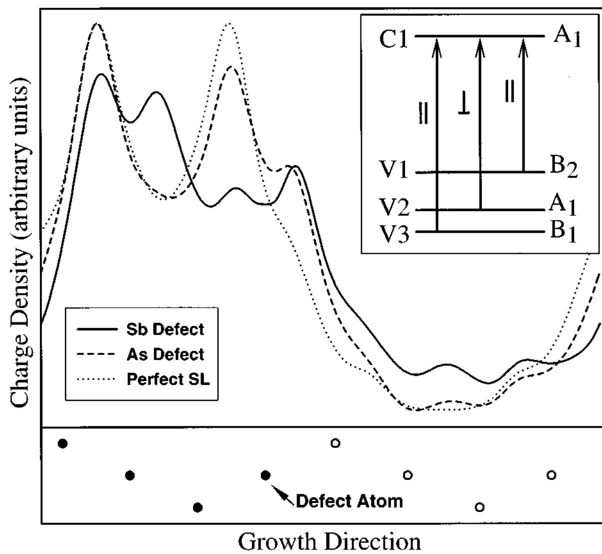

FIG. 6. The charge densities of the lowest conduction state ($C1$) at the Brillouin-zone center, integrated over the plane parallel to the interfaces, is plotted for the perfect superlattice, and for structures containing antimony and arsenic defects. The positions of the atom planes in the perfect structure are shown, solid circles representing Si planes, open circles Ge planes. The plane of the substitutional defects is also indicated. The inset is a schematic diagram illustrating the selection rules for transitions to $C1$ in the perturbed structures.

B. Conduction state perturbations

Now let us consider how the superlattice conduction states will be perturbed by the introduction of the antimony and arsenic defects. In the perfect Si_4Ge_4 superlattice the lowest conduction states originate from the zone folding of the Si X valleys oriented along the growth axis, and are confined to the Si layer. Figure 6 shows the charge density of this state, integrated over the unit cell in the plane parallel to the interfaces, compared to the charge densities of the corresponding states in the structures containing antimony and arsenic defects. The positions of the planes of atoms in the perfect structure are shown, and the plane in which the defects are placed is indicated.

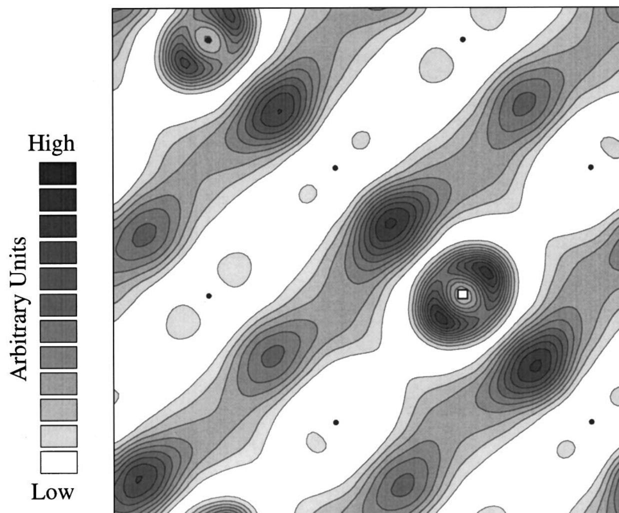

FIG. 7. The charge density (arbitrary units) of the second conduction state of a germanium defect in the Si_4Ge_4 superlattice, plotted in the plane parallel to the interfaces. The solid circles represent projections of the Si atoms which lay in the plotting plane prior to relaxation, and the open box shows the position of the defect atom.

From Fig. 6 we can see quite clearly that the lowest conduction state is very strongly perturbed by the antimony defect as compared to the arsenic. This is consistent with the findings of our studies of the defect resonances, providing further evidence of the strong coupling between the antimony defect and the lattice. Our calculations indicate that this disturbance is greater in the case of the antimony defect. One particular effect due to the presence of these defects is a reduction in the symmetry of the wave functions, clear from Fig. 6. This relaxes the selection rule which forbids all transitions to the lowest conduction state from the valence-band edge in a perfect Si_4Ge_4 superlattice. The inset to Fig. 6 indicates the revised selection rules for the defect structures, all of the transitions shown being forbidden in the perfect case. The interaction of defects with the interfaces themselves thus represents a mechanism for the alteration of the electronic structure of the heterostructures in such a way as to change the optical transitions. However, this belongs to a different class of problems, and lies outside the scope of the present study.

C. Germanium impurities

Finally, we also investigated the effect of a single Ge atom in the Si layer adjacent to the Si/Ge interface. As might be expected, the effect of the Ge defect was generally far less significant than that of the group-V donor defects discussed above. Indeed, the lowest conduction state is virtually identical to the perfect superlattice. However, the second conduction state exhibits a strong localization at the defect atom. The charge density of this state is plotted in Fig. 7 in the plane parallel to the interfaces. The existence of this degree of localization of the electron charge is interesting, since it is often assumed that the case of Ge defects in Si can be treated as one of an alloy. Figure 7 suggests that it is not appropriate to consider this material simply as a ''virtual-crystal alloy.'' Since the presence of Ge atoms in the Si layers is important in many real systems, arising through interface disorder, islanding, and diffusion, the question of how to model these systems is of some significance. We have shown that when the full microscopic properties of the interfaces are included, Ge defects demonstrate a behavior beyond that predicted by simple alloy models.

IV. CONCLUSION

To conclude, we applied *ab initio* pseudopotentials to a study of commonly occurring defects at the interfaces of Si/Ge heterostructures. These calculations provide us with a detailed description of the phenomena originating from bonds in the interface region itself—in what might be termed the intraface parameter space — which we have shown to play an important role in the behavior of the defects. In particular, our results have shown that the antimony defect interacts strongly with the Si/Ge interfaces, giving rise to

interface-related localized resonances and large local perturbations to the electronic structure of the superlattice. We have also demonstrated that the presence of Ge defects leads to localization. The microscopic defect-interface interaction thus represents a fresh parameter space in which experimental observables such as optical spectra or carrier scattering might be discussed.

ACKNOWLEDGMENTS

We would like to thank the U. K. Engineering and Physical Science Research Council, and the Office of Naval Research (U.S.A.) for financial support. We also thank the High Performance Computing Initiative for use of the Cray T3D at Edinburgh.

[1] See, e.g., M. Jaros, *Strained-Layer Superlattices,* edited by T. Pearsall, Semiconductors and Semimetals Vol. 32 (Academic, New York, 1990), p. 175, and references within.

[2] H. Presting, H. Kibbel, M. Jaros, R. J. Turton, U. Menzigar, G. Abstreiter, and H. Grimmeiss, Semicond. Sci. Technol. **7**, 1127 (1992).

[3] J. Engvall, J. Olajos, H. Grimmeiss, H. Kibbel, and H. Presting, Phys. Rev. B **51**, 2001 (1995).

[4] M. Gail, G. Abstreiter, J. Olajos, J. Engwall, H. Grimmeiss, H. Kibbel, and H. Presting, Appl. Phys. Lett. **66**, 2978 (1995).

[5] G. Bauer, J. Li, and E. Koppensteiner, J. Cryst. Growth **157**, 61 (1995).

[6] M. Jaros and A. W. Beavis, Appl. Phys. Lett. **63**, 669 (1993).

[7] R. J. Turton and M. Jaros, Semicond. Sci. Technol. **8**, 2003 (1993).

[8] G. B. Bachelet, D. R. Hamann, and M. Schlüter, Phys. Rev. B **26**, 4199 (1982).

[9] R. Jones, J. Phys. C **21**, 5735 (1988).

[10] M. J. Shaw, P. R. Briddon, and M. Jaros, Phys. Rev. B **52**, 16 341 (1995).

[11] See M. Jaros, *Deep Levels in Semiconductors* (Adam Hilger, Bristol, U.K., 1982).